THE ASTROPHYSICAL JOURNAL, 456:329–336, 1996 January 1

STELLAR MODELS AND LUMINOSITY FUNCTIONS FOR THE POPULATION II MAIN SEQUENCE DOWN TO ITS LOWER END

FRANCESCA D'ANTONA[1] AND ITALO MAZZITELLI[2]
Received 1995 March 16; accepted 1995 June 8

ABSTRACT

We have computed new sets of stellar models, for masses from $\sim 0.8\ M_\odot$ down to the lower termination of the main sequence, for metallicities and helium contents adequate to represent the halo and globular cluster populations, with the most updated opacity tables.

By means of theoretical color-$T_{\rm eff}$ transformations by Kurucz and by Allard, we have derived M_I versus $V-I$ data to be compared with globular clusters and nearby subdwarf data. We show that the characteristic "double kink" shape of the M_I versus $V-I$ diagram is well reproduced by the models, although better agreement would have been obtained if the $V-I$ theoretical colors were redder by ~ 0.1 mag.

We then discuss the mass-luminosity relation, particularly in correspondence with the kinks, since they turn out to be critical in establishing the luminosity functions (LFs) of the observed sets of stars. We present tables of the mass–M_I–$V-I$ relations, which can be used for comparisons with observed LFs.

We also discuss the general features of the luminosity functions obtained from these models assuming simple analytic mass functions of different power-law slope. We find that all the LFs peak in the range $8 \leq M_I \leq 10$, the magnitude of the maximum increasing both with Z and with the power-law exponent in the mass function. As an example, we compare our results with the recent *Hubble Space Telescope* observational results by Paresce et al. for the globular cluster NGC 6397.

Subject headings: stars: interiors — stars: low-mass, brown dwarfs — stars: luminosity function, mass function — stars: Population II — subdwarfs

1. INTRODUCTION

In order to gather information on the baryonic dark matter budget of our Galaxy, we require a good theoretical understanding of the structure of very low-mass main-sequence stars (VLMs), since the mass-luminosity (ML) relation is necessary in deriving the mass function (MF) from the observed LFs of stellar systems.

Most observational work to date has been devoted to Population I VLMs; more recently, new interest in Population II structures has been stimulated by two independent types of observations:

1. The *Hubble Space Telescope* (*HST*) is now producing new sets of data on the color-magnitude diagram of the lower main sequence of globular cluster (GC) stars. Further, the *HST*-based LFs for these systems are not biased any more by crowding, so that the observed LFs directly correlate with the MF. As GCs span more than a decade in metallicity, we must be ready to extend to the lower main sequence the comparison of principal sequences in the HR diagram and in the LFs plane, as is generally done when discussing turnoffs and horizontal branches.

2. The improved efficiency of CCD-based parallax determinations has produced an extended set of absolute magnitudes for nearby subdwarfs (Monet et al. 1992), in addition to the data from the photographic parallax program of the USNO. A first LF for subdwarfs has recently been derived by Dahn et al. (1995). Interpretation of the HR diagram and LF of subdwarfs is then a primary goal for stellar modelers, since the luminosities of these stars provide an important benchmark for establishing the distance moduli of GCs.

From the present MF of GCs, and correcting for the evaporation of low-mass stars during the lifetimes of the clusters, we can even gather, in the end, information on the way in which the fragmentation processes operated at the beginning of the life of our Galaxy.

In this work we elucidate the results of our new computations of stellar structure models that are adequate for comparisons with GCs and halo dwarfs. The models are constructed from $\sim 0.8\ M_\odot$ down to the hydrogen burning minimum mass, and we study the dependence of the minimum main-sequence luminosity and color on the metallicity.

Further, we apply color transformations and compare the results with observations. General features of the predicted LFs are shown, together with a comparison with the LF of NGC 6397 (Paresce et al. 1995).

2. THE THEORETICAL MODELS

Recently, Mazzitelli, D'Antona, & Caloi (1995, hereafter MDC) approached a global study of the ages of GCs by providing updated sets of horizontal branch and turn-off (TO) main-sequence (MS) models for several chemical compositions. The present work extends the computations to smaller mass MS structures; some minor modification in the input physics has been performed, to deal better with the problems encountered in the VLMs. A short discussion of the main physical features relevant for these stellar models follows.

2.1. *Input Physics and Numerics*

The models have been computed by means of the ATON code (Mazzitelli 1989), whose main features in the input physics, in the treatment of convection, and in the numerics are described in D'Antona & Mazzitelli (1994), and in MDC with

[1] Osservatorio Astronomico di Roma, I-00040 Monte Porzio, Italy.
[2] Istituto di Astrofisica Spaziale, C.P. 67, I-00044 Frascati, Italy.

special emphasis on the computation of Population II stellar models.

We adopt the Canuto & Mazzitelli (1991, 1992) model for overadiabatic convection, in the approximation described in MDC. Note, however, that on the lower MS overadiabaticity is only of minor relevance, and similar results would have been obtained with mixing length theory.

MDC adopted Kurucz (1991) opacities at $T \leq 6000$ K, and OPAL (Rogers & Iglesias 1992 and 1993, according to the solar Z-distribution by Grevesse & Noels 1993) at higher temperatures. Kurucz's opacities, however, do not include molecules, and are not adequate at the low $T_{\rm eff}$'s reached by VLMs. We then switched to opacities especially computed for this project by Alexander (1994; see Alexander & Ferguson 1994).

The differences between models integrated by adopting either Kurucz's or Alexander's opacities are quite small at $M \geq 0.4\ M_{\odot}$. For completeness, we also recomputed the models for the largest masses, to provide a homogeneous set of results.

It is to be noticed that structures close to the low-mass end of the MS cross a region in the ρ-T diagram not covered by the opacity tables, which are then extrapolated until electron conduction takes over. This uncertainty should not seriously affect our results, however, since the low-mass stars are completely convective and, as already noted, almost adiabatic. The case is different when opacities are extrapolated in the *optical atmosphere* (see below).

Thermodynamics deserves some discussion, since it is a relevant item for these structures. As in MDC, it follows Rogers, Swenson, & Iglesias (1995; see also Rogers 1994) for 5000 K $\leq T \leq 10^8$ K; Däppen et al. (1988) for $T \leq 5000$ K, and Magni & Mazzitelli (1979) elsewhere (that is, mainly in the high-ρ, low-T regions not covered by the other tabulations). Due to the relatively large densities and low temperatures in the external layers of low-mass MS stars, regions covered by the latter equation of state (EOS) are frequently met in the structures studied here, particularly in the partial ionization regime, where the value of the adiabatic temperature gradient is a key ingredient in determining the location of the star in the HR diagram.

Saumon (1994) has recently rediscussed a number of EOS for the nonideal gas regime, especially in the light of the EOS recently obtained by their group (see Saumon, Chabrier, & van Horn 1995) with an extremely careful and physically updated free-energy minimization technique. He found that, while the EOS by Magni and Mazzitelli fit with good accuracy his results far from ideal gas conditions and in the partial ionization regime (with respect to other thermodynamic treatments also available in the literature), there was instead a trivial error in the adiabatic gradient at low densities and large temperatures, in the range where radiation pressure takes over. Actually, the error was due to the scarcity of computer time when the first release of the EOS was generated ($\sim$1973), which forced the authors to use a coarse grid outside the nonideal gas conditions, ultimately leading to bad numerical derivatives. The mistake has been long since corrected, and is in any case absent in the present computations, since the ρ-T regions in question are now covered by the EOS from Rogers et al. What is worth noting instead is that the present EOS, in nonideal gas regions, is largely consistent with the more recent results by Saumon et al.

However, to better investigate possible inconsistencies between our EOS and Saumon's, we computed a pure-hydrogen structure of 0.2 $M_{\odot}$. We then compared the pressures taken from our model to those of Saumon, along the ρ-T track corresponding to the subatmospheric layers. We found differences of the order of 1%–2% (that is, of the order of the precision of interpolation in the tables) for log $T \leq 4.3$, but these increased to a maximum of 15% around log $T = 4.5$ (our pressures being lower than Saumon's), and then the differences decreased again so as almost to vanish in the complete ionization regime. The physical reason for these differences is in the fact that, due to the use of more updated potentials in the short-range molecular interactions, Saumon still finds some H_2 molecules (and thus larger pressures due to non ideal gas effects, e.g., excluded volume) where we already find almost complete molecular dissociation.

Since the thickness of this region, in which our EOS can possibly underestimate pressure and incorrectly estimate other thermodynamic variables, is small even if compared with the subatmospheric layers only; and since the differences with the recent EOS are quite small, we conclude that, from the thermodynamical point of view, our results are reasonably consistent with those which would be obtained from Saumon's EOS.

Nuclear cross sections are from Harris et al. (1983); weak and intermediate screening (the latter, in low-mass stars, directly affects even the p-p chain) from Graboske et al. (1973).

2.2. *Input Chemistry*

As in MDC, we explored a set of parameters which are considered "standard" in GC evolution. As for helium, we assumed the conventional lower limit for the helium mass fraction $Y = Y_{\rm BigBang} = 0.23$ (e.g., Audouze 1986). We set the CNO abundances at the solar ratios (Grevesse & Noels 1993), neglecting a possible enhancement of oxygen and other α elements. In the present case, this may affect the $T_{\rm eff}$ determination since, according to Salaris, Chieffi, & Straniero (1993), a track with standard CNO composition may in fact simulate tracks for α-enhanced mixtures, if a properly evaluated, larger *equivalent* total metal content is chosen. We will come back to this last point during the comparisons with the observations, which will be performed with *equivalent* metal mass-fraction Z. The helium abundances have been adjusted to the metallicities, according to the hypothesis $\Delta Y/\Delta Z \sim 2 \pm 0.5$, based on the assumption of $Y_{\odot} = 0.27$.

2.3. *Atmospheric Structure*

This is possibly the least updated physical input, since we adopt as boundary conditions a gray atmosphere with a $T(\tau)$ relationship. The atmospheric integration is stopped at $\tau = \frac{2}{3}$, and from that point on, full integration of the structure equations is performed. For stars having thin atmospheric envelopes, the procedure is safe as long as the atmosphere is completely radiative (Baraffe et al. 1995) and *inside* the ρ-T boundaries of the opacity tables. When convection begins to extend also into the optical layers, the gray-atmosphere approximation becomes progressively less and less satisfactory. Ultimately, the nonideal gas opacity is the missing physical input that keeps us from a better understanding of the brown dwarfs (D'Antona 1987).

Given that our observables are log $L/L_{\odot}$ and $T_{\rm eff}$ for each mass, we then require correlations $T_{\rm eff}$ versus color and bolometric corrections to compare our results with observations. In MDC we adopted Kurucz's (1993) transformations to V, $B-V$ as these are the most commonly used data for TO and HB stars. As V, $V-I$ are the most interesting colors for describing

TABLE 1

MODELS FOR $Z = 10^{-4}$, $Y = 0.23$, $T = 10$ GYR

$M/M_\odot$	log $L/L_\odot$	log $T_{\rm eff}$	M_I	$V-I$
0.825	0.353	3.828	3.448	0.542
0.800	0.189	3.820	3.838	0.574
0.750	−0.070	3.798	4.422	0.657
0.700	−0.290	3.775	4.906	0.743
0.600	−0.698	3.722	5.788	0.950
0.500	−1.085	3.670	6.678	1.194
0.400	−1.369	3.649	7.374	1.315
0.350	−1.474	3.643	7.635	1.355
0.300	−1.588	3.639	7.918	1.382
0.250	−1.728	3.633	8.266	1.421
0.200	−1.917	3.625	8.739	1.476
0.170	−2.072	3.619	9.129	1.521
0.150	−2.207	3.613	9.470	1.566
0.130	−2.388	3.603	9.927	1.638
0.120	−2.518	3.592	10.284	1.692
0.110	−2.712	3.570	10.833	1.791
0.100	−3.063	3.509	11.728	2.124
0.097	−3.285	3.472	12.138	2.375

the VLMs of both Populations I and II, we decided to provide transformations into those quantities. In § 4 we discuss the correlations that we used: we took advantage of Kurucz's BC's and $T_{\rm eff}$–$V-I$ correlations down to 4000 K, and supplemented them with the models of Allard & Hauschildt (1995a) for lower $T_{\rm eff}$'s.

2.4. *The Luminosity Functions*

We predicted the LFs for coeval systems of ages $t_0 = 10$ and 15 Gyr, adopting a mass function ($dN/d\log M$) of the form:

$$\frac{dN}{d\log M} = kM^{-x},$$

and show results for LFs evaluated using

$$\frac{dN}{d\log L/L_\odot} = \frac{dN}{d\log M} \times \left(\frac{d\log M}{d\log L/L_\odot}\right)_{t_0}. \quad (1)$$

3. THE SHAPE OF THE HR DIAGRAM IN POPULATION II

Tables 1–4 collect the relevant results for each chemistry. Mass, log $L/L_\odot$, $T_{\rm eff}$, M_I, and $V-I$ are given. Figure 1 shows

TABLE 2

MODELS FOR $Z = 10^{-3}$, $Y = 0.235$, $T = 10$ GYR

$M/M_\odot$	log $L/L_\odot$	log $T_{\rm eff}$	M_I	$V-I$
0.800	0.092	3.800	3.991	0.639
0.750	−0.140	3.782	4.519	0.706
0.700	−0.346	3.761	4.978	0.784
0.600	−0.747	3.702	5.873	1.021
0.500	−1.146	3.643	6.835	1.375
0.400	−1.456	3.620	7.600	1.546
0.350	−1.569	3.614	7.882	1.591
0.300	−1.683	3.610	8.166	1.621
0.250	−1.825	3.604	8.520	1.665
0.200	−2.015	3.597	9.013	1.712
0.170	−2.169	3.590	9.424	1.755
0.150	−2.300	3.583	9.778	1.797
0.120	−2.600	3.562	10.605	1.915
0.110	−2.779	3.541	11.123	2.041
0.100	−3.058	3.500	11.920	2.489
0.098	−3.143	3.484	12.189	2.719
0.096	−3.244	3.466	12.518	3.010
0.094	−3.385	3.440	13.000	3.480

TABLE 3

MODELS FOR $Z = 2 \times 10^{-3}$, $Y = 0.24$, $T = 10$ GYR

$M/M_\odot$	log $L/L_\odot$	log $T_{\rm eff}$	M_I	$V-I$
0.800	0.017	3.788	4.130	0.680
0.750	−0.198	3.772	4.624	0.740
0.700	−0.397	3.749	5.066	0.826
0.650	−0.591	3.722	5.502	0.932
0.600	−0.789	3.689	5.965	1.090
0.550	−0.990	3.654	6.453	1.304
0.500	−1.177	3.633	6.912	1.459
0.450	−1.344	3.618	7.326	1.573
0.400	−1.486	3.609	7.679	1.641
0.350	−1.603	3.603	7.970	1.685
0.300	−1.719	3.599	8.272	1.715
0.250	−1.862	3.593	8.653	1.758
0.200	−2.055	3.584	9.171	1.820
0.150	−2.340	3.570	9.937	1.910
0.120	−2.635	3.547	10.761	2.046
0.110	−2.800	3.530	11.227	2.217
0.105	−2.907	3.518	11.530	2.346
0.102	−2.986	3.507	11.772	2.493
0.100	−3.050	3.497	11.980	2.645
0.098	−3.126	3.484	12.242	2.863
0.096	−3.216	3.467	12.579	3.181
0.095	−3.267	3.458	12.771	3.356
0.094	−3.323	3.447	12.993	3.569
0.093	−3.387	3.434	13.267	3.864
0.092	−3.467	3.419	13.615	4.173

TABLE 4

MODELS FOR $Z = 4 \times 10^{-3}$, $Y = 0.24$, $T = 10$ GYR

$M/M_\odot$	log $L/L_\odot$	log $T_{\rm eff}$	M_I	$V-I$
0.800	−0.127	3.770	4.423	0.746
0.750	−0.319	3.751	4.859	0.819
0.700	−0.502	3.726	5.274	0.921
0.650	−0.687	3.697	5.704	1.058
0.600	−0.879	3.664	6.172	1.257
0.550	−1.067	3.635	6.638	1.464
0.500	−1.237	3.618	7.061	1.594
0.450	−1.394	3.605	7.451	1.693
0.400	−1.529	3.597	7.813	1.761
0.350	−1.646	3.591	8.134	1.813
0.300	−1.763	3.585	8.455	1.864
0.250	−1.911	3.579	8.852	1.912
0.230	−1.982	3.576	9.042	1.935
0.200	−2.106	3.570	9.378	1.979
0.180	−2.205	3.564	9.652	2.022
0.150	−2.391	3.553	10.162	2.096
0.130	−2.563	3.541	10.639	2.186
0.120	−2.678	3.532	10.958	2.288
0.115	−2.747	3.526	11.152	2.356
0.110	−2.829	3.519	11.381	2.435
0.108	−2.865	3.515	11.490	2.489
0.105	−2.928	3.509	11.676	2.571
0.102	−3.001	3.500	11.908	2.707
0.100	−3.061	3.491	12.113	2.850
0.098	−3.132	3.479	12.379	3.063
0.096	−3.216	3.464	12.716	3.349
0.095	−3.263	3.454	12.930	3.537
0.094	−3.313	3.444	13.158	3.729
0.093	−3.367	3.433	13.418	3.951
0.092	−3.427	3.421	13.728	4.164
0.091	−3.493	3.408	14.065	4.384
0.090	−3.530	3.401	14.248	4.500

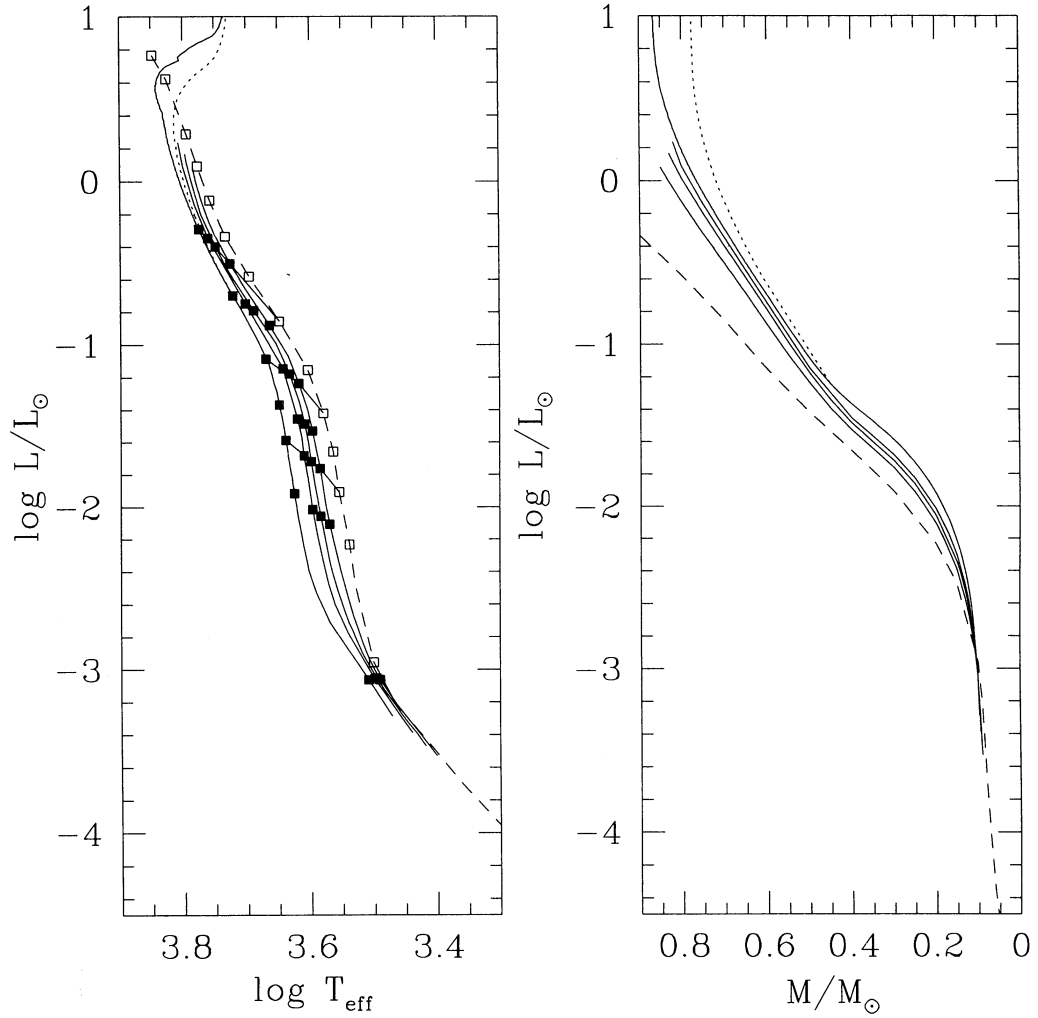

FIG. 1.—Left panel shows the HR diagram for the models computed in this paper. From left to right, metallicities are $Z = 10^{-4}$, $Z = 10^{-3}$, $Z = 2 \times 10^{-3}$, $Z = 4 \times 10^{-3}$. Models of masses from 0.7 to 0.1 $M_{\odot}$ are marked, and 0.7, 0.5, and 0.3 $M_{\odot}$ models are connected for clarity. All the continuous lines are for an age of 10 Gyr, while the dotted one refers to $Z = 10^{-4}$ and 15 Gyr. Models for Population I (from D'Antona & Mazzitelli 1994, " CM Alexander " set at $t = 10^9$ yr) (*dashed line*) are shown for comparison, with masses from 1.4 to 0.1 $M_{\odot}$ indicated as open squares. The right panel shows the mass-luminosity relations, where lower curves correspond to increasing metallicities. The dotted line again refers to $Z = 10^{-4}$ and 15 Gyr, while the dashed line represents the Population I models. Notice how there is a correspondence between the double kink in the HR diagram and the changes of slope in the ML relations.

the theoretical HR diagram on the left and the corresponding ML relation on the right. Also for solar chemistry the MS location and the ML relation at an age of 10^9 yr are given, for comparison, from D'Antona & Mazzitelli (1994).

All the Population II MSs display a "double kink" shape (i.e., two changes of slope), whose observational counterpart has been recently found in the GC NGC 6397 (Paresce et al. 1995). The more luminous kink is to be attributed to the already well-understood drop in the values of the adiabatic gradient close to the surface, when the structure begins crossing the H_2 molecular dissociation region (Copeland, Jensen, & Jorgensen 1970). The decreased gradient makes the surface of the star hotter (and slightly more luminous) than it would have been without the H_2; from this point on, the MS shows a steeper slope in the HR diagram, and *the ML relation flattens.*

The steepness of the MS below the first kink, being a function of the adiabatic gradient, depends on the equation of state adopted. Bergbusch & VandenBerg (1992) performed similar computations with a different EOS, and with enhanced O abundance. When comparing their results with the present ones at *equivalent* metal abundance (Fig. 2) we see that, on the average, the agreement is quite satisfactory, the slope of the MS being somewhat steeper in the present case. This is consistent with the more sophisticated and complete treatment of the nonideal gas effects in our EOS, which force a larger recombination, and a lower adiabatic gradient.

The adiabatic gradient remains quite low in the H_2 dissociation and in the joint H-ionization regions, until the mass decreases to $\sim 0.12\ M_{\odot}$. At this point, degeneracy appears and quickly takes over in a range of only $\sim 0.03\ M_{\odot}$. This forces the MS to suddenly approach a nearly constant-radius track in the HR diagram, at lower and lower luminosities (and $T_{\rm eff}$'s). The second kink appears.

A phenomenological picture of the process can be described as follows: when $T_{\rm eff}$ drops below ~ 3000 K, recombination is almost complete at the surface, and the atmospheric opacity decreases. This leads to larger and larger pressures at the photospheric boundary, and in the whole structure, as the

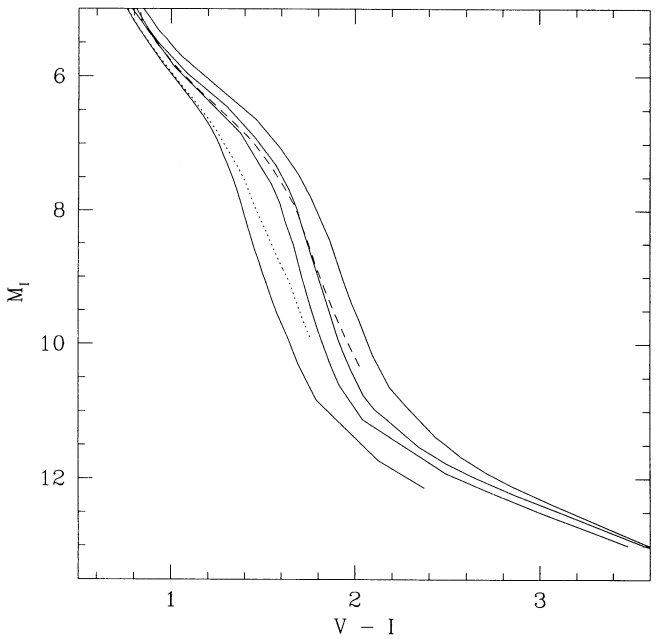

FIG. 2.—Comparison of our model location in the M_I–$V-I$ diagram with the models of Bergbusch & VandenBerg (1992). All models have been transformed into the observational plane by employing the color relations of the present study. The dotted line refers to their models with $[M/H] = -2.26$, the dashed one to models with $[M/H] = -1.3$. These models have large oxygen enhancement, so that they must be compared with our models of larger metallicity.

mass of the star decreases further. The average adiabatic gradient resumes rising, since the edge of *pressure* ionization (which takes over *temperature* ionization) is very narrow. Because the gradient increases, $T_{\rm eff}$ decreases faster, and the central pressure (density) increases, leading to degeneracy and fast decline of luminosity with mass.

The precise location of the second kink is therefore a function of the atmospheric opacities, which determine the thermal structure of these stars. For larger metal abundances it can occur at lower $T_{\rm eff}$, but the global morphology of the HR diagram (the double kink) is the same for any chemical composition.

As shown in Figure 1, when the structures approach the second kink, the ML relation *steepens*, both due to the average increase in $\nabla_{\rm ad}$ and since, at the same time, the nuclear energy output is fading away.

In the lower part of the diagram the curves for all the compositions almost merge, including the Population I curve; this shows that the models close to the bottom of the MS are located practically *along a constant radius track* ($R \lesssim 0.1\ R_\odot$) in the HR diagram, as already discussed above. A detailed comparison with the data of the lower end of the main sequence of NGC 6397 (Paresce et al. 1995) is hampered by the fact that the *HST* color they adopt is not a standard $V-I$: in fact, while the m_{814} magnitude should quite closely correspond to I the m_{606} does not correspond to V. Nevertheless, keeping the suggestion coming from the shape of the diagram, we find that, among all stars redder than the second kink, the difference in mass cannot be larger than $0.02\ M_\odot$: quite a small range of masses, covering a large region in the HR diagram!

4. THE TRANSFORMATIONS INTO THE OBSERVATIONAL PLANE

Comparisons of our models with observations requires transformation of $T_{\rm eff}$'s and $\log L/L_\odot$ into magnitudes and colors; this is not a trivial task for M dwarfs. Kurucz (1993) made available transformations of this kind down to 3500 K. He provided both BC_V and $V-I$, so that it is possible to convert theoretical data into M_I or M_V and $V-I$. There are two problems with Kurucz's correlations: first, for $T_{\rm eff} = 3750$ and 3500 K the colors become bluer and the BCs become smaller than at 4000 K, and this is surely unrealistic. Further, the lower end of the MS extends down to $T_{\rm eff} \sim 2500$ K and below, so that we need to supplement Kurucz's correlations with data from other atmospheric models available in the literature. For this purpose, we adopted correlations from the "Base model grid" by Allard & Hauschildt (1995a).

Figure 3 shows the comparison between Kurucz's and Allard's BCs and $V-I$ for metal abundance $[M/H] = -2$ ($Z \sim 2 \times 10^{-4}$), after correcting the BC's for the zero-point difference between the two sets of computations. The fit between the two sets of models is not completely satisfactory, since it fails by ~ 0.2 mag at $T_{\rm eff} = 4000$ K, and the differences seems to increase with decreasing $T_{\rm eff}$. The reasons for this discrepancy cannot be easily traced back, but are probably due to intrinsic problems inherent in the physical inputs in these models (computation of opacities and EOS including molecules, treatment of convection in the optical atmosphere, radiative transfer in nonideal gas conditions, etc.) so that, for $V-I \gtrsim 2$, uncertainties of about 0.2 mag or even more can still be present in the comparisons that result. The situation will probably be better when the "NextGen" grid of models by Allard & Hauschildt (1995b) is available.

To avoid discontinuities, we decided simply to adopt Kurucz's correlations down to $T = 4000$ K and Allard's for

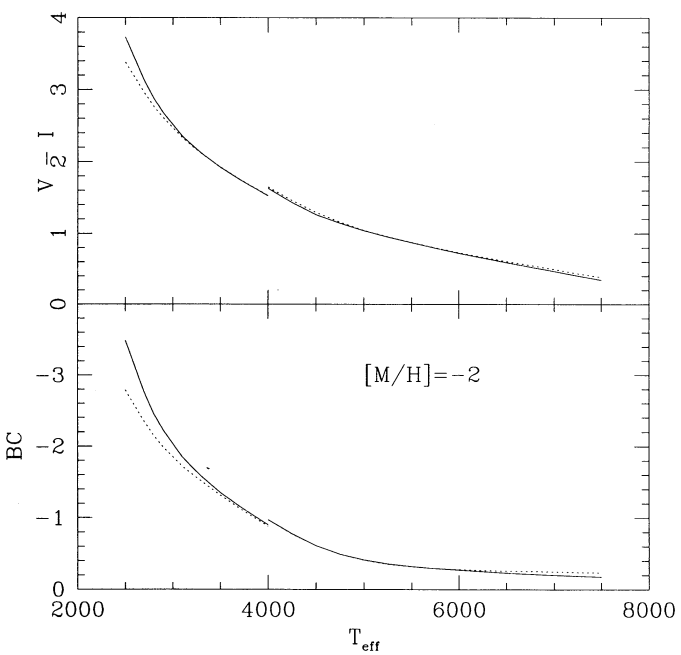

FIG. 3.—Comparison between Kurucz's ($T_{\rm eff} \geq 4000$ K) and Allard's ($T_{\rm eff} \leq 4000$ K) BCs and $T_{\rm eff}$–$V-I$ correlations for $[M/H] = -2$, $\log g = 4$ (*solid lines*) and 5 (*dotted line*).

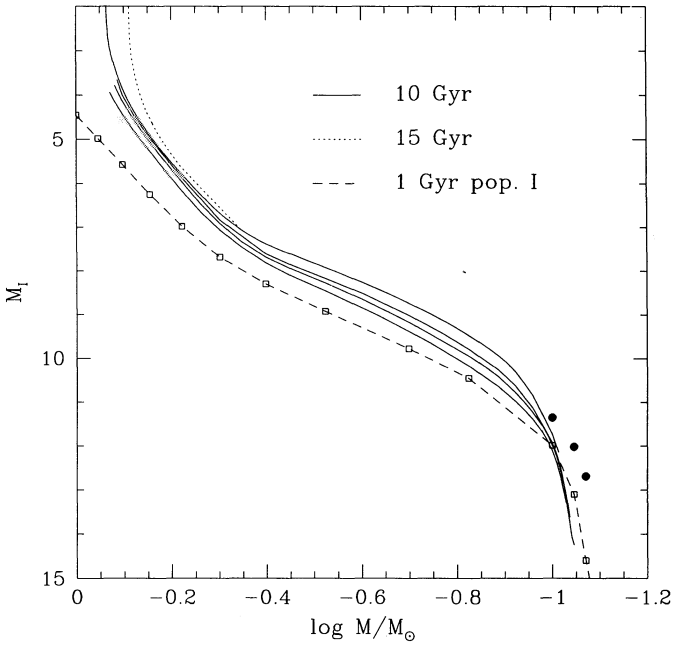

FIG. 4.—Mass-M_I magnitude relations for different chemistries, the lines from top to bottom refer to increasing metallicities, ending with the Population I relation from D'Antona & Mazzitelli (1994) (age 10^9 yr, *open squares and dashed line*). All the Population II models refer to an age of 10 Gyr, while the $Z = 10^{-4}$ composition provides also the relation for age of 15 Gyr (*dotted line*). The three full points represent the models by Baraffe et al. (1995) for $[M/H] = -1.5$, $Y = 0.275$.

$T \leq 3500$, and to linearly interpolate in between. In view of the intrinsic uncertainties above quoted, it is in fact useless to devise more elaborate interpolation schemes.

5. COMPARISONS WITH OBSERVATIONS IN THE HR DIAGRAM

In Figure 4 we show the mass-M_I relations, and in Figure 5 we compare our transformed HR-diagram loci in the M_I–$V-I$ diagram with some data from the literature, namely, the parallax star sample from Monet et al. (1992), and the TO MS data exhibited for NGC 6752 by Bolte et al. (1994). For this latter cluster, we assumed a distance modulus $(m - M)_I = 13.35$, and dereddened in $V-I$ by -0.02 mag.

Our sequences provide a reasonable match for the HR diagram location of both the GC data and of the subdwarfs of Monet et al. In particular, we stress the fact that the double kink shape shown by the theoretical models has a clear observational counterpart: the first kink is defined by the GC HR diagram, the second one is instead clearly defined by the nearby subdwarfs with $V-I \gtrsim 2$.

If our interpretation is correct, the lowest-luminosity subdwarfs of Monet et al. also define *the Population II bottom of the MS* in the range $2 \leq V-I \leq 3$. According to our preceding discussion on the theoretical models, the range of masses in this color interval should not exceed a very few hundreds of $M_\odot$. Thus, even if models predict that stable models of $Z \geq 10^{-3}$ should exist at $V-I \geq 3$, the probability of finding subdwarfs with such colors is very low.

The theoretical models which best describe the location of NGC 6752 stars and the subdwarfs of Monet et al. are those with metallicities $Z = 10^{-3}$ and 2×10^{-3}, while the metallicity of NGC 6752 is somewhat smaller ($Z \sim 5 \times 10^{-4}$—Webbink 1985) and also some of the subdwarfs of Monet et al. may be more extreme in metal content. Remember, however, that we have not assumed an O-enhancement, so our values of Z should be viewed as *equivalent* metallicities (see Salaris et al. 1993). The fact that the present models tend to overestimate the metal abundances of the observed samples of stars is consistent with those stars having significant enhancements in the abundances of the α elements.

It was our purpose to compare our results also with the theoretical ones of Baraffe et al. (1995), for which no bolometric luminosities, but only magnitudes and colors are provided, since the authors employ non-gray atmospheric models in their computations. Unfortunately, they also adopt for Population II a helium abundance $Y = 0.275$, and this alone can be responsible for large differences with respect to our models. In Figure 4 we also show the low end of the MS from Baraffe et al. for a metal abundance $[M/H] = -1.5$ ($Z \sim 6 \times 10^{-3}$) (*black dots*). These latter models are definitely more luminous than ours, but this is simply the effect qualitatively expected for a larger He-abundance. So, while we do expect that the use of non-gray atmospheres would lead to significant differences in the modeling of very low mass stars (whose internal structure is largely affected by the optically thin layers—see D'Antona 1987), we are not able to quantify these differences.

Figure 5 also contains some more interesting information. First, models predict that, at the lowest levels of luminosity in the field subdwarf sequence, the reddest stars should be also the more metal-rich ones. This comes out from inspection of Tables 1–4 with attention to the lowest mass models. The minimum main-sequence mass and luminosity is more of academic than practical interest: increasing the opacities, when Z increases, these shift from $\log L/L_\odot = -3.285$ for the 0.097 $M_\odot$ model of $Z = 10^{-4}$ to $\log L/L_\odot = -3.467$ for the 0.092

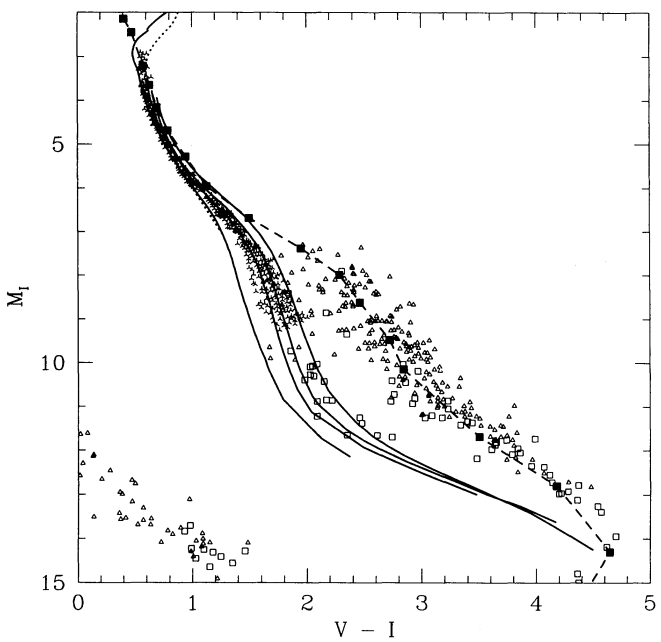

FIG. 5.—M_I vs. $V-I$ diagram including Monet et al.'s 1992 dwarfs and subdwarfs (*open squares and small triangles*), and the sketched NGC 6752 diagram from Bolte et al. (1994) (*three-pointed stars*), placed at the cluster distance $(m - M)_I = 13.35$, taking into account reddening and absorption $[\delta(V-I) = -0.02]$. The double kink shape is reproduced in the observations: Monet subdwarfs (at $V-I \geq 2$) define the second after-kink region.

$M_\odot$ model of $Z = 4 \times 10^{-3}$. More interestingly, these models at the ends of the sequences span a large range in $V-I$: so it is more probable to find subdwarfs of larger metallicity at colors $V-I \gtrsim 2.5$. (This value is obviously very uncertain; it depends quite a lot on the adopted transformations $T_{\rm eff}$–$V-I$.)

Further, the *very small* mass difference for the entire sequence of the stars of Monet et al. in the color range $2.1 \leq V-I \leq 2.8$ has a related consequence for the luminosity function of these objects. (The recent determination of the halo stars LF by Dahn et al. (1995) indicates that the LF flattens at $M_V \sim 12$, corresponding to $M_I \sim 10$, as expected from these models—see § 6.) This is a point we want to emphasize: since the mass-luminosity relation is extremely steep in this region, its convolution with a MF having *almost any* power law exponent, will provide a luminosity function showing a maximum around $M_I \sim 9$–10 (or $M_v \sim 11$–12), and a decline at larger magnitudes.

As we will soon show, in fact, the slope of the low end of the luminosity function carries little information about the mass function, being mainly driven by the steepness in the mass-luminosity relation.

6. THE LUMINOSITY FUNCTION

We present in Figure 6 the theoretical LFs obtained from our models for several power-law indices ($x = 0$, $x = 0.5$, and $x = 1$) of the mass function.

As anticipated above, the slope of the LF at $10 \lesssim M_I \lesssim 12$ has little to do either with the MF slope or with the metallicity: it mainly reflects the slope of the ML relation in this range. The maximum value of the LF and the magnitude where it occurs are instead related to x. This means that if we want to derive MF of a distant cluster, we must know its distance modulus with good accuracy. If, for instance, we overestimate the distance modulus, we get a shallower MF than the real one (D'Antona 1995).

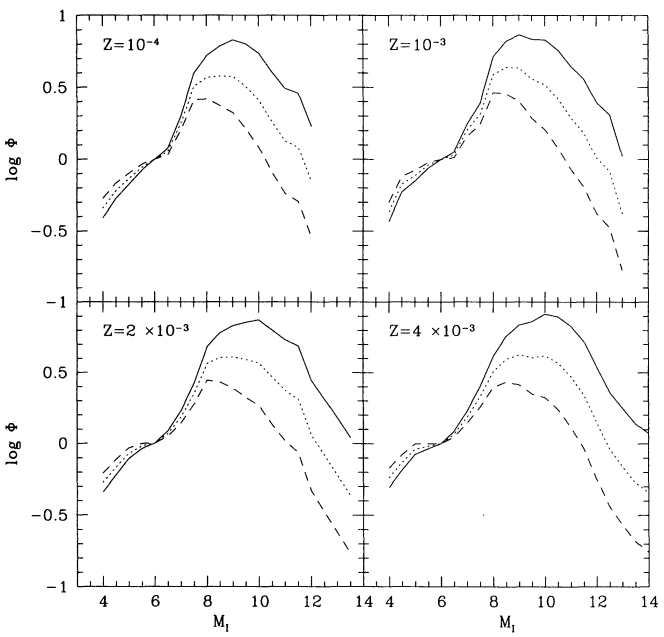

FIG. 6.—Theoretical LFs for the four chemistries, corresponding to MFs with $x = 1$ (*solid line*), $x = 0.5$ (*dotted line*), and $x = 0$ (*dashed line*). All the LFs have been normalized at $M_I = 6$. Notice how the slope in the M_I range 10–12 is almost independent of the metallicity and of the MF index: it mainly depends on the slope of the mass-luminosity relation.

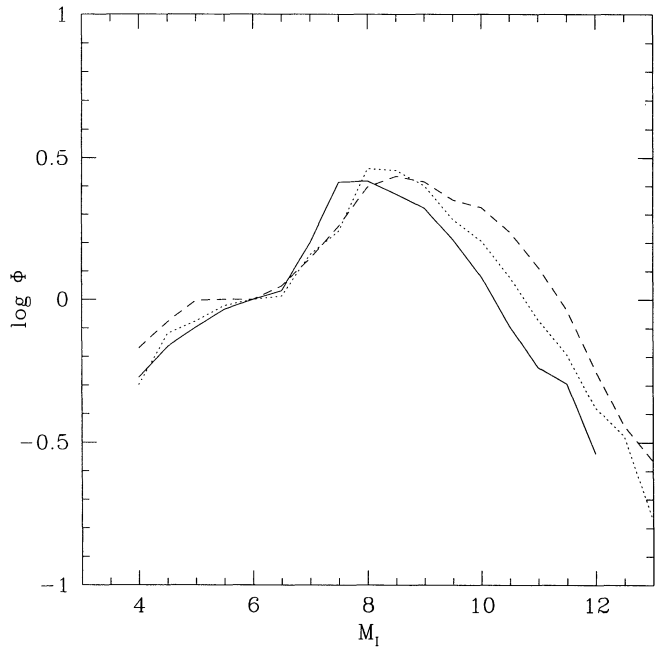

FIG. 7.—Theoretical LFs for $x = 0$ and metallicities $Z = 10^{-4}$ (*solid line*), $Z = 10^{-3}$ (*dotted line*), and $Z = 4 \times 10^{-3}$ (*dashed line*). The shift of the maximum in the LF with increasing metallicity is evident.

In Figure 7 we show how the peak of the LF shifts to fainter magnitudes when the metallicity increases: GCs with larger Z will have the maximum at fainter M_I. Again, exact knowledge of the distance modulus is necessary, since the maximum is not sharply peaked, and its dependence on Z, although evident, is not striking. This effect due to metallicity seems to have been observationally revealed when comparing the LFs of the GCs NGC 6397 ($Z \sim 10^{-4}$) and 47 Tuc ($Z \sim 4 \times 10^{-3}$) (De Marchi 1995).

Figure 8 shows the effect of age on the LF. Evolutionary effects begin to be present at $M_I \sim 4.5$, so that knowledge of the entire LF from the turnoff down to ~ 6 magnitudes below may help in discriminating the age of the globular cluster studied.

Keeping in mind the above warnings, we performed a test comparison of our results with a set of observed data. We again call the reader's attention to the fact that use of our LFs requires caution, because uncertainties still exist in the stellar models, and in the transformations into the observational plane.

We chose, for comparison, the LF of NGC 6397 (Paresce et al. 1995). As for the distance modulus, a canonical value in the visual is $(m-M)_v = 12.3$ (Fahlman et al. 1989). Assuming a ratio of interstellar absorption, between the I and V band, $A_I/A_V = 0.48$ (Rieke & Lebofsky 1985) and given that the cluster is reddened by $E(B-V) = 0.18$ (Webbink 1985), the I distance modulus should be $(m-M)_I = 12$. However, for consistency we derive from our new HB models (MDC 1995) a value $(m-M)_v = 12.55$, from which $(m-M)_I = 12.3$.

From Figure 9 one sees that, with this distance modulus, and for a metal abundance between $Z = 10^{-4}$ and $Z = 10^{-3}$, a relatively shallow MF ($x \sim 0$) seems to fit the observations reasonably. The fit can probably be made more accurate by

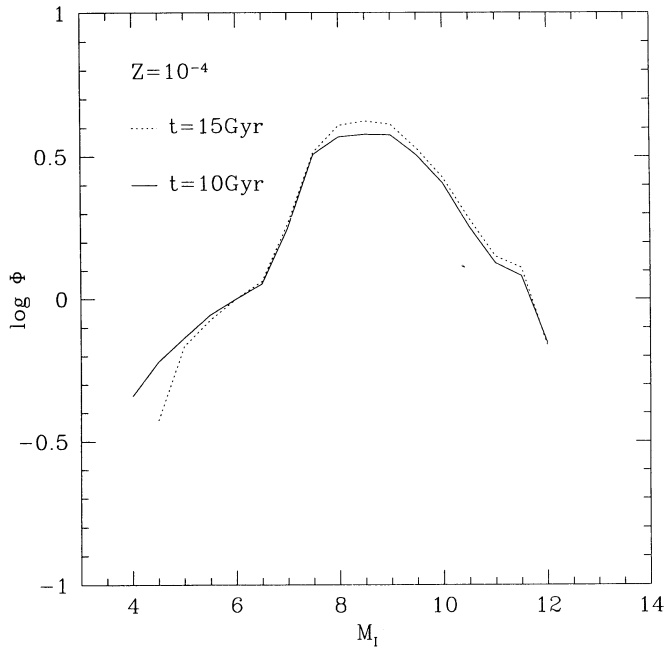

FIG. 8.—LFs for $x = 0.5$ and ages 10 and 15 Gyr. Evolutionary effects begin to be present at $M_I \sim 4.5$. Knowledge of the entire LF from the turn-off down to ~6 magnitudes below may help in discriminating the age of the globular cluster.

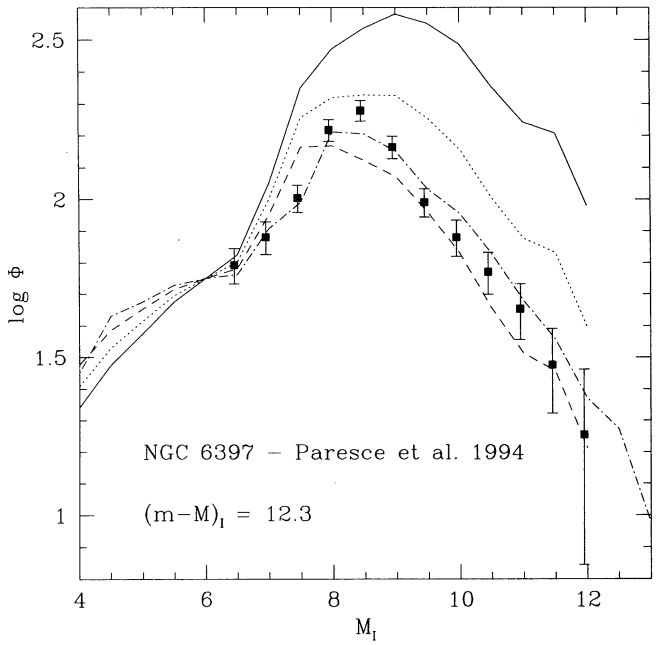

FIG. 9.—Theoretical LFs compared with Paresce et al. (1995) LF for NGC 6397, adopting a canonical distance modulus $(m - M)_I = 12.3$ (see text). The $Z = 10^{-4}$ LFs for $x = 0$ (*dashed line*), $x = 0.5$ (*dotted line*) and $x = 1$ (*solid line*) are shown. The $Z = 10^{-3}$, $x = 0$ LF is also shown.

(arbitrarily) adjusting the distance modulus and/or the metal abundance, but our opinion is that the uncertainties already present in this kind of comparison do not justify procedures of fine tuning.

7. CONCLUSIONS

From our low-mass stellar models, we find that the lower end of the main sequence for metal-poor populations must show a "double kink" morphology, which is clearly present in observed samples. By means of the mass-luminosity relation, we also derive the lower MS theoretical luminosity functions for various metal abundances and spectral indices of the mass function. By comparisons with NGC 6397 photometry, we conclude that the present mass function for this globular cluster is quite shallow (power-law index $0 \leq x \leq 0.5$).

We thank all the researchers who made this work possible by sending us or allowing us access to their results, in particular Dave Alexander, France Allard, Bob Kurucz, Werner Däppen, Dimitri Mihalas, Forrest Rogers, and Don VandenBerg. France Allard is also thanked for detailed information about her models. Finally, we warmly thank an anonymous referee and Ivan King for language-editing the manuscript.

REFERENCES

Alexander, D. R. 1994, private communication
Alexander, D. R., & Ferguson, J. W. 1994, ApJ, 437, 879
Allard, F., & Hauschildt, P. H. 1995a, ApJ, 445, 433
———. 1995b, ApJ, submitted
Audouze, J. 1986, in Nucleosynthesis and Chemical Evolution, ed. B. Hauch, A. Maeder, & G. Meynet (Geneva: Geneva Obs.), 429
Baraffe, I., Chabrier, G., Allard, F., & Hauschildt, P. H. 1995, ApJ, 446, 35
Bergbusch, P. A., & VandenBerg, D. A. 1992, ApJS, 81, 163
Bolte, M., Hesser, J. E., Stetson, P. B., & VandenBerg, D. 1994, NOAO Newsletter, June, 4
Burrows, A., Hubbard, W. B., Saumon, D., & Lunine, J. I. 1993, ApJ, 406, 158
Canuto, V. M., & Mazzitelli, I. 1991, ApJ, 370, 295
———. 1992, ApJ, 389, 724
Copeland, H., Jensen, J. O., & Jorgensen, H. E. 1970, A&A, 5, 12
Dahn, C. C., Liebert, J., Harris, H. C., & Guetter, H. H. 1995, in The Bottom of the Main Sequence and Beyond, ed. C. G. Tinney (Berlin: Springer), 239
D'Antona, F. 1987, ApJ, 320, 653
———. 1995, in The Bottom of the Main Sequence and Beyond, ed. C. G. Tinney (Berlin: Springer), 13
D'Antona, F., & Mazzitelli, I. 1994, ApJS, 90, 467
Däppen, W., Mihalas, D., Hummer, D. G., & Mihalas, B. W. 1988, ApJ, 332, 261
De Marchi, G. 1995, private communication
Fahlman, G. G., Richer, H. B., Searle, L., & Thompson, I. B. 1989, ApJ, 343, L49
Graboske, H. C., DeWitt, H. E., Grossman, A. S., & Cooper, M. S. 1973, ApJ, 181, 457
Grevesse, N., & Noels, A. 1993, in Origin and Evolution of the Elements, ed. N. Prantzos, E. Vangioni-Flam, & M. Cassé (Cambridge: Cambridge Univ. Press), 14
Harris, M. J., Fowler, W. A., Caughlan, G. R., & Zimmermann, B. A. 1983, ARA&A, 21, 165
Kurucz, R. L. 1991, in Stellar Atmospheres: Beyond the Classical Models, ed. L. Crivellari, I. Hubeny, & D. G. Hummer (Dordrecht: Kluwer), 441
———. 1993, unpublished data
Magni, G., & Mazzitelli, I. 1979, A&A, 72, 134
Mazzitelli, I. 1989, ApJ, 340, 249
Mazzitelli, I., D'Antona, F., & Caloi, V. 1995, A&A, in press (MDC)
Monet, D. G., Dahn, C. C., Vrba, F. J., Harris, H. C., Pier, J. R., Luginbuhl, C. B., & Ables, H. D. 1992, AJ, 103, 638
Paresce, F., De Marchi, G., & Romaniello, M. 1995, ApJ, 440, 216
Rieke, G. H., & Lebofsky, M. J. 1985, ApJ, 288, 618
Rogers, F. J. 1994, in IAU Colloq. 147, The Equation of State in Astrophysics, ed. G. Chabrier & E. Schatzman (Cambridge: Cambridge Univ. Press), 16
Rogers, F. J., & Iglesias, C. A. 1992, ApJ, 397, 717
———. 1993, ApJ, 412, 572
Rogers, F. J., Swenson, F. J., & Iglesias, C. A. 1995, ApJ, in press
Salaris, M., Chieffi, A., & Straniero, O. 1993, ApJ, 414, 580
Saumon, D. 1994, in IAU Colloq. 147, The Equation of State in Astrophysics, ed. G. Chabrier & E. Schatzman (Cambridge: Cambridge Univ. Press), 306
Saumon, D., Chabrier, G., & van Horn, H. M. 1995, ApJS, 99, 713
Webbink, R. F. 1985, in IAU Symp. 113, Dynamics of Star Clusters, ed. J. Goodman & P. Hut (Dordrecht: Reidel), 541